

Article

Photoelectrocatalytic Hydrogen Production Using a TiO₂/WO₃ Bilayer Photocatalyst in the Presence of Ethanol as a Fuel

Panagiotis Marios Adamopoulos, Ioannis Papagiannis, Dimitrios Raptis and Panagiotis Lianos *

Department of Chemical Engineering, University of Patras, 26500 Patras, Greece; cmng3238@upnet.gr (P.M.A.); ion.papg@gmail.com (I.P.); dgraptis86@yahoo.gr (D.R.)

* Correspondence: lianos@upatras.gr; Tel.: +30-2610-997513

Received: 13 September 2019; Accepted: 19 November 2019; Published: 21 November 2019



Abstract: Photoelectrocatalytic hydrogen production was studied by using a photoelectrochemical cell where the photoanode was made by depositing on FTO electrodes either a nanoparticulate WO₃ film alone or a bilayer film made of nanoparticulate WO₃ at the bottom covered with a nanoparticulate TiO₂ film on the top. Both the electric current and the hydrogen produced by the photoelectrocatalysis cell substantially increased by adding the top titania layer. The presence of this layer did not affect the current-voltage characteristics of the cell (besides the increase of the current density). This was an indication that the flow of electrons in the combined semiconductor photoanode was through the WO₃ layer. The increase of the current was mainly attributed to the passivation of the surface recombination sites on WO₃ contributing to the limitation of charge recombination mechanisms. In addition, the top titania layer may have contributed to photon absorption by back scattering of light and thus by enhancement of light absorption by WO₃. Relatively high charge densities were recorded, owing both to the improvement of the photoanode by the combined photocatalyst and to the presence of ethanol as the sacrificial agent (fuel), which affected the recorded current by “current doubling” phenomena. Hydrogen was produced under electric bias using a simple cathode electrode made of carbon paper carrying carbon black as the electrocatalyst. This electrode gave a Faradaic efficiency of 58% for hydrogen production.

Keywords: WO₃; TiO₂; hydrogen production; photoelectrocatalysis

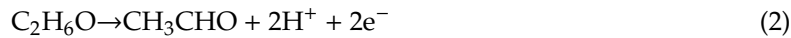
1. Introduction

Photoelectrocatalytic hydrogen production is one of the most popular research subjects because it promises an effective route for converting solar energy and storing it as chemical energy in the form of hydrogen. The popularity of hydrogen stems from the fact that it has the highest gravimetric heat of combustion (~286 kJ/mole), while its combustion leads to the production of water. Hydrogen is mainly produced by reforming of fossil fuels. It can also be produced by electrolysis using, for example, renewable electricity. Theoretically, 1.23 V are necessary to split water by electrolysis; however, in reality, much higher voltages and expensive electrocatalysts are necessary. In this sense, water splitting by photoelectrocatalysis [1] is a very promising approach since it necessitates much lower electric biases. However, oxidation of water is a four-electron process:

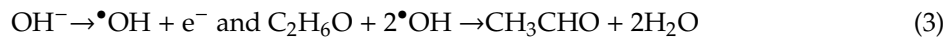


Therefore, it is necessary to simultaneously extract four units of charge in order to oxidize water and produce molecular oxygen. This is not easy and necessitates oxygen evolution co-catalysts. On the

contrary, it is easier to oxidize an organic substance. For example, in the case of ethanol, oxidation leads to the formation of acetaldehyde, which is a two electron process, therefore easier to realize, either directly [2–4]:



or by the intermediate of hydroxyl radicals:



For most organic substances, oxidation and subsequent mineralization proceed by steps, as in the above case of ethanol, which usually are two electron processes, therefore easier to oxidize than water. In terms of oxidation potential, oxidation of ethanol to acetaldehyde corresponds to -0.21 V [5], i.e., it is much lower than the above mentioned potential of 1.23 V necessary to oxidize water. Molecular hydrogen production by reduction of protons or water is also a two electron process [3,4]:



or



Therefore, photoelectrocatalytic hydrogen production by using an organic substance as a fuel is even more of a promising approach, which has been adopted in the present work.

The standard configuration of a photoelectrocatalytic cell for hydrogen production involves a photoanode electrode carrying a semiconductor photocatalyst and a cathode electrode where reductive reactions are carried out, producing hydrogen. Both electrodes are immersed in an electrolyte, which increases the internal cell conductivity and provides the ionic species necessary to allow device functioning in a cyclic manner [3,4]. Figure 1 shows a simplified design of a photoelectrocatalysis cell. When photons are absorbed by the photocatalyst, electron-hole (e^- - h^+) pairs are generated. Holes are consumed by oxidation reactions, such as (2) or (3), while electrons move through an external circuit and are consumed by reduction reactions at the cathode. The overall result of oxidation and reduction can be represented, for example, by combining (2) or (3) with (4) or (5), respectively [2]:



which describes the consumption of ethanol, from now on referred to as the “fuel”, to produce hydrogen by means of a photoelectrocatalytic process. Acetaldehyde may be further oxidized until complete mineralization and further hydrogen production. The complete mineralization of ethanol may be expressed by the following overall reaction [3,4]:



which is the same as ethanol reforming [6] and can be rightfully called “photoelectrocatalytic alcohol reforming”.

Photoelectrocatalysis necessitates then the presence of a photocatalyst. There exists a rich literature on the choice of photocatalysts [4,7,8]. Researchers searching for a new photocatalyst have developed resourceful arguments in their favor; however, it is a matter of fact that very few among them simultaneously possess more than one quality that distinguishes each one of them from the others. Nanostructured titania is the best such example, but WO_3 is also a distinguished choice as well [9–11]. Titania is an n-type, low cost, non-toxic semiconductor, easy to process, and having a strong adhesive quality on various types of electrodes. It possesses a strong oxidative potential (about 3 V in the case of anatase) and a conduction band conveniently located with respect to the hydrogen production potential (about -0.2 V vs. NHE) [12]. Titania also possesses relatively large charge carrier mobility. For example, its hole diffusion length is of the order of 10^4 nm, much larger than that of WO_3 (~ 150 nm) and

hematite (2–4 nm) [13]. These properties would make titania an ideal photocatalyst; however, it still suffers from substantial electron-hole recombination, while its light absorption range is limited only to the UV. Nanoparticulate tungsten oxide is also a very popular choice, and thanks to its substantial range of visible light absorption, it has been studied for several decades [11,14–17] as an alternative to the UV absorbing titania. Indeed, WO_3 has a bandgap ranging between 2.5 and 2.8 eV, and it may thus absorb light up to 500 nm, which accounts for 12% of the solar radiation on the surface of the Earth [17]. WO_3 is an n-type indirect semiconductor. It is easy to synthesize and deposit on electrodes; it has a moderate hole-diffusion length (~ 150 nm [17], as already said); it is resistant against photocorrosion; and it is stable at relatively low pH values. For this reason, WO_3 has been studied as a photoanode material for photoelectrochemical water splitting applications [11,14–20]. Its valence band is located approximately at +2.8 V vs. NHE [12]; therefore, it also possesses high oxidative power, and it is well placed for water and organics' oxidation. Its conduction band is located at positive potentials (approximately +0.2 to +0.3 V vs. NHE, cf. [12]); therefore, it is located substantially lower than that of titania. If the two semiconductors are then brought into contact, it is expected that photogenerated electrons may be transferred from TiO_2 to WO_3 , thus achieving charge separation and limiting $e^- - h^+$ recombination. However, it is understood that since the photon absorption spectral range for titania is limited, its role as an electron source for WO_3 is of limited importance. There is another role that titania may play, which is of utmost importance, and this is the passivation of surface states of WO_3 that a top cover of titania can offer. This role will be investigated in the present case.

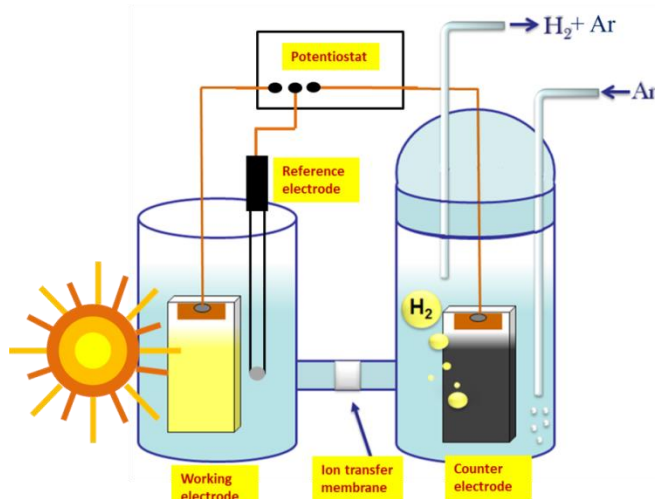


Figure 1. Schematic representation of the reactor employed in the present work, showing the working electrode (photoanode), counter electrode (cathode electrode carrying an electrocatalyst), reference electrode, and connections with a potentiostat, which provides the necessary bias. Hydrogen production is monitored in a de-aerated environment obtained by Ar flow.

In addition to the surface states' passivation effect, there is one more reason to enhance WO_3 's performance. As will be discussed below, contrary to the transparent WO_3 layer, the top titania layer is a light scattering film, which scatters back to WO_3 at least part of the incident light. This situation supports conditions for enhancement of light absorption by the WO_3 layer, and this, of course, results in higher photocurrent production.

Unbiased flow of electrons from the photoanode to the cathode electrode would necessitate a substantial potential difference between the two electrodes. The potential of the photoanode is roughly defined by the conduction band of the photocatalyst, while that of the cathode electrode by the redox potential of the reduction reaction. In the case of hydrogen production, the potential in a strongly acidic environment is around 0 V vs. NHE. The conduction band of titania lies at about −0.2 V vs. NHE, as already said. This difference of 0.2 V is too small, and it is eliminated by losses. It is even worse in

the case of WO_3 , which has a conduction band slightly more positive than the hydrogen production potential. Therefore, no unbiased flow of electrons is expected for a WO_3 photoanode and is hardly expected in the case of a TiO_2 photoanode. In other words, when the above two photocatalysts are used, production of hydrogen may be obtained only by applying a bias. This is the reason that in the present work, hydrogen was produced under electric bias, as schematically illustrated in Figure 1.

By taking into account the above knowledge, in the present work, we are studying photoanodes made by combining nanoparticulate WO_3 with nanoparticulate TiO_2 , in a bilayer structure comprising a bottom film made of WO_3 and a top film made of TiO_2 , in order to investigate the merits of such a combination. Measurements have focused on photoelectrocatalytic hydrogen production by using ethanol as the model fuel [19] with the understanding that other organic materials, either biomass byproducts or water soluble pollutants, may apply as well [20].

2. Results and Discussion

In the present work, as already said, the photoanodes were made either by deposition of a WO_3 nanoparticulate film alone on an FTO electrode or by adding a layer of nanoparticulate titania on the top. As seen in Figure 2A, WO_3 nanoparticles were polydisperse with the size ranging between 20 and 50 nm. The BET specific surface area was $26 \text{ m}^2 \text{ g}^{-1}$, and X-ray diffractograms (not shown) revealed the formation of monoclinic WO_3 crystallites of size around 25 nm as calculated by using Scherrer's formula. The quantity of WO_3 in the film was approximately 4.5 mg cm^{-2} . When the titania layer was added on the top, a complete coverage of the lower WO_3 film was obtained by exposing only the titania film. The SEM image of the film in Figure 2B then showed a typical titania nanostructure. The quantity of titania was approximately 4 mg cm^{-2} . The latter maintained the characteristics previously described in other publications [21,22]. The thickness of the combined semiconductor film was approximately determined by its scanning electron microscope profile, and it was below 1 μm .

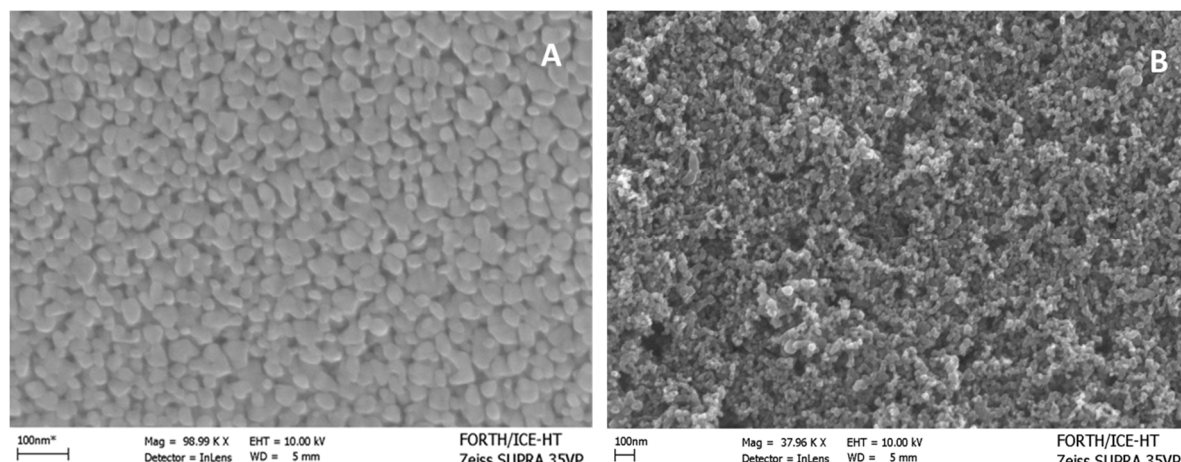


Figure 2. FE-SEM images of a WO_3/FTO (A) and a $\text{TiO}_2/\text{WO}_3/\text{FTO}$ (B) film.

The spectroscopic characteristics of the WO_3 film before and after titania deposition are shown in Figure 3A. WO_3 film alone absorbed light up to about 480 nm, i.e., within a spectral range typical of this semiconductor. When titania was added on the top, the reflectance-absorption spectrum presented a different aspect depending on which side of the film was exposed to light. When the light passed through the transparent FTO electrode (cf. Figure 3B), the spectrum (Curve 2) showed similar characteristics as those of WO_3 alone (Curve 1). Since the photoanode operates by this mode (Figure 3B), it was seen that the spectroscopic characteristics of WO_3 prevailed. When absorption was recorded by front reflection, i.e., by means of the top titania layer, the corresponding curve (Curve 3) had a typical aspect of a nanocrystalline titania film. This is an additional indication of complete coverage of the WO_3 layer by (the light scattering) titania.

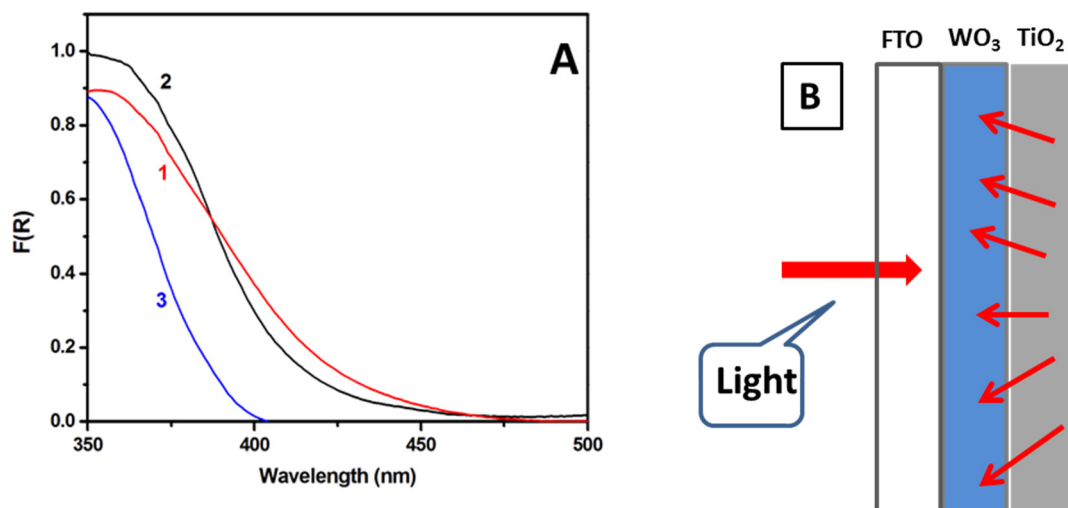


Figure 3. (A) Reflection-absorption spectra of the WO_3 (1) and the TiO_2/WO_3 (2,3) photoanode. Curve 3 was obtained by front side reflection and Curve 2 by reflection through the supporting FTO glass. Curve 3 is typical of the nanoparticulate titania absorption spectrum. (B) Graphical representation of the direction of photons in the presently used setup.

The presence of TiO_2 on the top of WO_3 was expected to encourage electron-hole separation, thanks to the difference between the levels of the conduction band of these semiconductors, which may reach more than 0.4 V, with the titania conduction band being the more negative of the two (cf. the band levels in [23]). However, as already said, the role of titania as a sensitizer of WO_3 was expected to be limited since its photon absorption range was limited. On the contrary, deposition of titania on the top of the WO_3 film may result in the passivation of surface defects of the latter, and this would limit charge recombination sites. Passivation of surface defects has been observed and recorded in TiO_2/WO_3 and other semiconductor combinations [24–30]. In addition, titania films are more stable than WO_3 films; therefore, the top titania layer provided protection against aggressive electrolytes. Finally, the top titania layer provided a light scattering film, in contrast to the transparent WO_3 film, which may send light back to WO_3 , thus enhancing its capacity for photon harvesting. This is especially convenient in the present case where light was absorbed through the supporting FTO layer. This configuration is illustrated by the design of Figure 3B. Light scattering by the titania layer was due to the agglomeration of titania nanoparticles into large clusters (cf. Figure 2B).

The beneficial effects that the bilayer photocatalyst film had on the activity of the photoelectrocatalytic cell were immediately seen by recording current-voltage curves, as seen in Figure 4. More than a 30% increase of current was recorded when the titania layer was added on the top, compared with a photoanode made of WO_3 alone. The curves of Figure 4 were recorded under the same conditions, differing only by the composition of the photocatalyst film. The curves were recorded in light chopping mode demonstrating that the voltage range of pure photocurrent extended between about 0.2 and 1.8 volts vs. Ag/AgCl. The small anodic peak below this range was due to capacitance current deriving from the adsorption of cations from the electrolyte into the pores of the mesoporous film [21]. The increase of the dark current above 1.8 V vs. Ag/AgCl was due to electrolysis. The electrolyte was 0.5 M NaClO_4 with 5% v/v ethanol added in the anode compartment. In accordance with previous publications [19,20], in the absence of ethanol (not shown; cf. the data in [19]), lower currents were obtained in both photoanode cases. This was expected as previously explained [19,20]. Ethanol acted as a hole scavenger, which further limited charge recombination, thus resulting in higher currents. Moreover, transient species formed by ethanol oxidation induced current increase by the “current doubling” phenomenon [31]. Indeed, the maximum current density expected for a photoanode with light absorption threshold at 480 nm (cf. Figure 3A) was no more than 5 mA cm^{-2} [4]. However, the current density presently increased under bias well beyond this limit,

and this was rationalized only by the current doubling effect. The addition then of the titania layer and the presence of the fuel (ethanol) resulted in the production of substantial photocurrent.

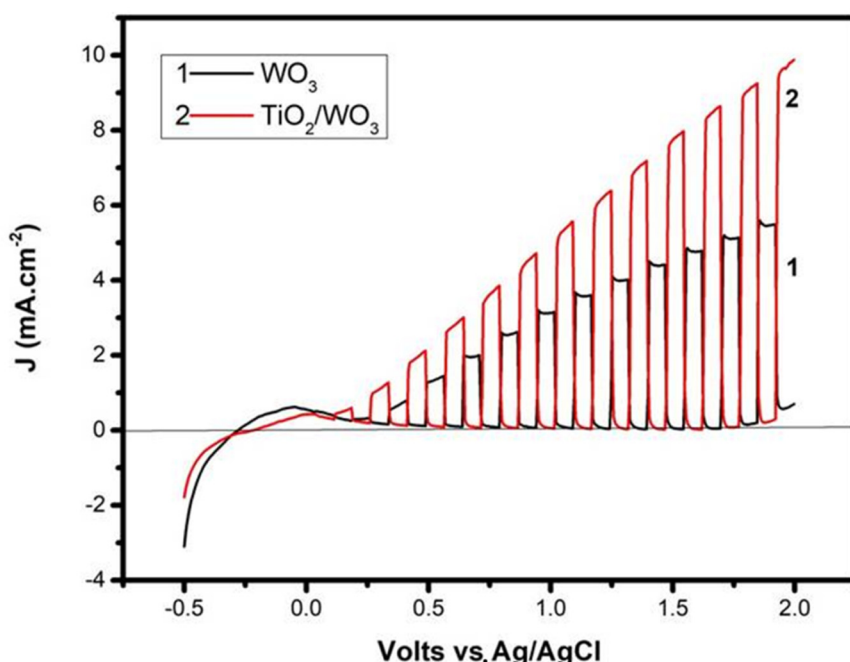


Figure 4. Current density-voltage curves for a photoelectrocatalytic cell made of two different photoanodes. Recording was done in light chopping mode demonstrating the voltage range of the pure photocurrent.

The increase of the current when titania was added on the top of WO_3 was not due to titania acting as the photocatalyst by itself. When a photoanode was made by using titania alone, by taking care to deposit the same quantity of photocatalyst (4 mg cm^{-2}), under the same conditions of the cell configuration and the electrolyte and fuel concentration, the behavior of the current-voltage curve presented a completely different aspect, as seen in Figure 5. The maximum current density was only 0.42 mA cm^{-2} , while in the case of Figure 4, the current increase was more than 3 mA cm^{-2} . Most importantly, open circuit voltage (the point where the current became zero) was $<-1 \text{ V}$ vs. Ag/AgCl , while in Figure 4, the open circuit voltage was approximately located at 0.0 V vs. Ag/AgCl . The difference in the onset potential between a WO_3 and a TiO_2 photoanode roughly reflected the difference in the electrochemical potential of each semiconductor, and it was systematically observed. The fact that the addition of titania on the top of WO_3 preserved the characteristics of the latter simply means that the bottom lying WO_3 layer defined the level at which electrons left the anode electrode. It was furthermore observed that in the case of titania alone, the photocurrent soon reached saturation by the voltage increase, while in the case of WO_3 and TiO_2/WO_3 , the current continuously increased with bias voltage. In other words, the addition of the titania layer on the top of WO_3 resulted only in a current increase without affecting the original appearance of the pure WO_3 current-voltage curve. Obviously, photogenerated electrons in the titania layer were transferred to the electrode only by means of the underlying WO_3 layer, and titania did not act as a photocatalyst by itself. Because of the continuous increase of current with increasing voltage and since hydrogen production was proportional to the current flowing through the external circuit of the cell, it was expected that the hydrogen production rate should strongly depend on the applied electric bias.

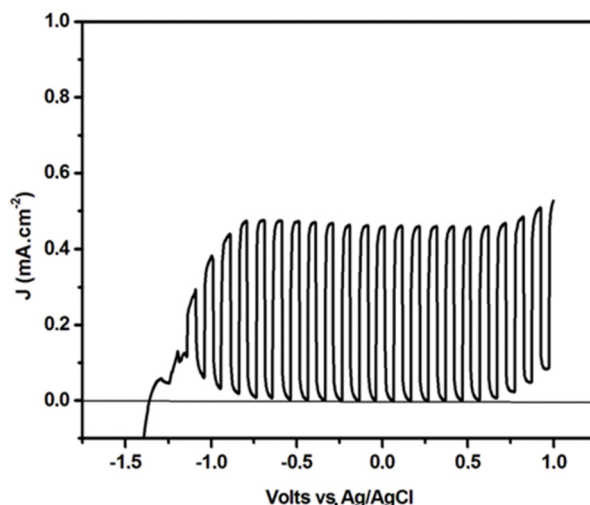


Figure 5. Current density-voltage curves for a photoelectrocatalytic cell made of a (pure) titania photoanode. Recording was done in light chopping mode demonstrating the voltage range of the pure photocurrent. The anodic rise at negative voltages is due to the capacitance current deriving from the adsorption of Na cations from the electrolyte solution [21].

At this point, a question arises about the fate of the photogenerated holes. An approximate positioning of band levels for TiO_2 and WO_3 nanoparticulate semiconductors and of the oxidation potentials of the three possible hole scavengers in the present system is presented by the diagram in Figure 6 (cf. also the band levels in [23]). Titania nanoparticles used for the present application were a mixture of anatase and rutile. For this reason, the valence band level could not be clear cut and was expected to lie between 3.0 and 2.8 V vs. NHE. A similar situation existed for WO_3 due to the fact that its bandgap may range between 2.5 and 2.8 eV, as already said. This created an uncertainty concerning the direction of the hole transfer. In Figure 6, we favored the transfer of holes to titania, which, being on the top, facilitated the interaction with hole scavengers in the solution. In view of structural imperfections in both semiconductors, it was hard to make a strong assertion on this matter. In any case, the level of 3.0 V vs. NHE was positive enough to produce $\cdot\text{OH}$ radicals. However, vast losses, again due to structural imperfections, may make transfer of holes to OH^- ions less probable than the most obvious hole scavenging by ethanol or water. Oxidation of ethanol, as already said, is easier than water therefore, ethanol remained the most probable hole consumer.

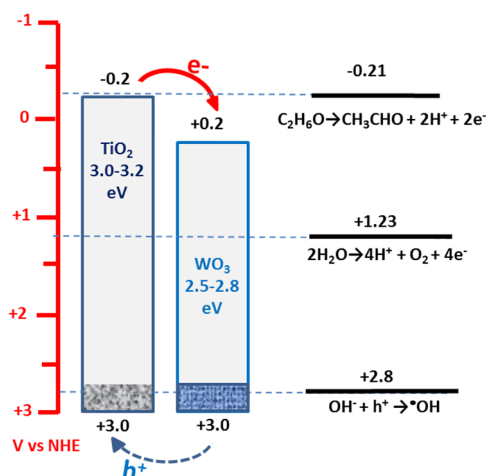


Figure 6. Approximate band levels for nanoparticulate TiO_2 and WO_3 and oxidation potentials of the possible hole scavengers in the present system.

The hydrogen production rate by employing the two types of photoanode was indeed monitored, and the results are presented in Figure 7. In Figure 7, we tried to demonstrate the strong variation of the hydrogen production rate as a function of the applied bias. No hydrogen production was observed without a forward bias. Three different electric biases were applied, chosen within the above photocurrent range. Thus, each curve was divided into three parts, one for each applied bias, as marked on the graph. Each part demonstrated a period of a rising rate followed by a period of a practically constant rate. A fast increase of the hydrogen production rate took place after changing the applied bias, and it corresponded to the filling of tubes and detection device with the additional hydrogen produced. The variation of the hydrogen production rate with applied bias was a clear demonstration that hydrogen produced by reduction reactions at the cathode depended on the current flowing through the external circuit of the cell. Indeed, by comparing Curve #2 of Figure 4 with Curve #2 of Figure 7, it is found that the hydrogen produced was roughly proportional to the current. In addition, the combined TiO_2/WO_3 photoanode produced a higher quantity of hydrogen than the WO_3 photoanode, in accordance with the higher current flow. The maximum hydrogen production rate recorded under the present conditions, with 1.6 V bias vs. Ag/AgCl, was $4.4 \mu\text{mol} \cdot \text{min}^{-1}$. The corresponding current was 24.3 mA. The Faradaic efficiency for hydrogen production under the present conditions could be calculated by the following equivalent [32]: 1 $\mu\text{mole}/\text{min H}_2$ corresponds to $(10^{-6} \text{ moles}) \times (6.022 \times 10^{23} \text{ molecules/mole}) \times (2 \text{ electrons/H}_2 \text{ molecule}) \times (1.6 \times 10^{-19} \text{ Coulomb/electron})/60 \text{ s}$, which is equal to 3.21 mA. Consequently, $4.4 \mu\text{mole} \cdot \text{min}^{-1}$ correspond to 14.1 mA. Since the average real current was 24.3 mA, then the Faradaic efficiency was 58% ($14.1/24.3 = 0.58$). The Faradaic efficiency depended on the device configuration and reactor parameters, as well as the efficiency of the cathode electrode and the quality of the electrocatalyst. The presently obtained value was relatively low, owed mainly to the use of an inexpensive electrocatalyst (carbon paper loaded with carbon black), but also to the fact that the reactor parameters were not optimized. Comparable Faradaic efficiencies were also obtained in a previous work [32]. It must be stressed at this point that the quality of the photoanode and the strength of the applied bias mainly dictated the flowing current, while the functionality of the cathode electrode mainly affected the Faradaic efficiency. It relied then mainly on the counter electrode to improve Faradaic efficiency, and this will be a matter of our future projects.

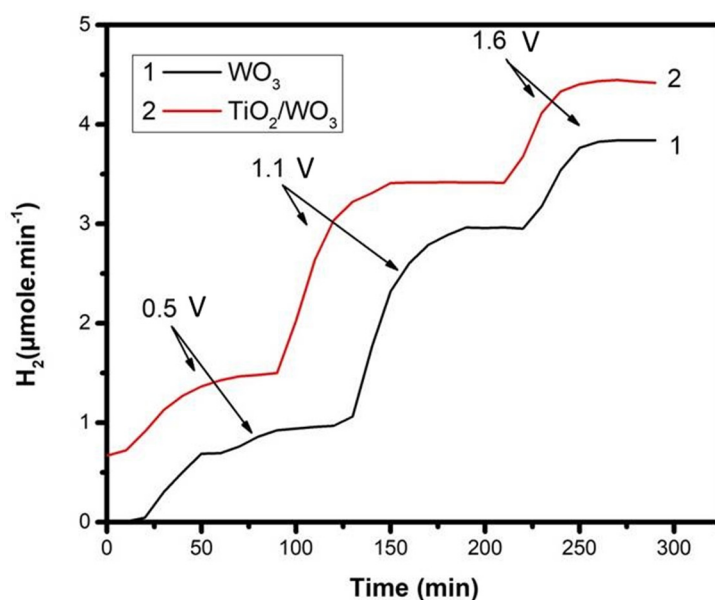


Figure 7. Variation of the photoelectrocatalytic hydrogen production rate by applying various electric biases. Biases are marked on the graph, and they are expressed in volts vs. Ag/AgCl electrode. The two curves correspond to the two photoanodes.

The data of Figure 7 corresponded to relatively short-time measurements. When the experiment was run for a longer period of time, a slow current drop was observed, which was accompanied by an analogous drop of the hydrogen production rate (cf. the data in our previous work [32]). The proportionality of current with the hydrogen production rate preserved the value of the Faradaic efficiency, in accordance with the above discussion. It was then again concluded that the photoanode and its immediate environment, as well as the applied bias dictated the current production, while the capacities of the counter electrode dictated the Faradaic efficiency for hydrogen production.

3. Materials and Methods

3.1. Materials

Reagents were obtained from Sigma Aldrich and were used as received. Millipore water was used in all experiments. $\text{SnO}_2:\text{F}$ transparent conductive electrodes (FTO, resistance 8 ohm/square) were purchased from Pilkington (Pilkington, Toledo, OH, USA) and carbon paper from SGL Technologies GmbH (Meitingen, Germany, thickness 190 μm), and carbon black was a donation from Cabot Corporation (Vulcan XC72, Billerica, MA, USA).

3.2. Construction of WO_3 Photoanodes

A quantity of 0.4 g of high purity tungsten powder (99.99%) with average particle sizes up to 10 microns reacted with 3 mL of 30% aqueous hydrogen peroxide [33] under sonication for 2–3 h until a transparent colorless solution was obtained. The excess of H_2O_2 was catalytically decomposed using a Pt foil [34,35] by keeping the mixture at 10 °C with a thermostated water bath. Then, the solution was mixed with 3 mL of ethanol and 0.3 g of the surfactant Triton X-100, and the mixture was deposited on previously cleaned FTO slides cut into the appropriate dimensions. FTO slides were cleaned first with soap and then by sonication in acetone, ethanol, and water. Deposition was made by spin-coating at 2000 rpm for 20 s. After depositing 3 subsequent layers, the obtained film was calcined for 10 min at 500 °C (heating rate of 20 °C/min). The procedure was repeated at least six times. This rather tedious procedure was necessary to make a compact film without voids. The active area of the film was 1 cm × 1 cm in the case when it was used for IV measurements. Larger films of 3.5 cm × 5 cm were employed for hydrogen production.

3.3. Preparation of the TiO_2 Paste and Deposition on the WO_3 Film

Deposition of titania on the top of the WO_3 film was achieved by using a paste made of commercial titania nanoparticles. The paste was prepared by modifying a previously published procedure [36]. Three grams of Degussa P25 powder were placed in a small mortar with 0.5 mL of acetic acid and carefully ground for 3 min. Then, 2.5 mL of triple-distilled water were added in 5 equal doses while grinding the mixture. Grinding continued by then gradually adding 10 times ethanol by 1 mL and subsequently 6 times by 1.25 mL. At the end of this procedure, a big amount of ethanol, almost 30 mL, was added, which helped to detach titania from the walls of the mortar. The mixture was then sonicated several times, for 2 s each time, until a homogeneous dispersion was obtained. Consequently, we added 10 g of 2-(4-methyl-1-cyclohex-3-enyl)propan-2-ol (terpineol) and repeated ultrasonication again until a homogeneous dispersion was obtained. Finally, we added an amount of ethyl cellulose (5% w/w) dissolved in EtOH (10% w/v) and again repeated ultrasonication to obtain a homogeneous mixture. The whole procedure lasted 50–60 min, and when it ended, the solution was ready for use. This paste can be condensed in a rotary evaporator; however, in the present work, it was used as is, in order to apply it by spin-coating. Indeed, titania was applied on either a WO_3 covered electrode or a plain FTO glass by spin-coating at 3000 rpm for 30 s.

3.4. Construction of the Counter Electrode

The counter electrodes that were used in the present work were made of carbon cloth on which a carbon black paste was deposited by the following procedure: 0.3 g of carbon black was mixed with 8 mL of distilled water by vigorous mixing in a mixer (more than 4000 r.p.m.) until it became a viscous paste. This paste was further mixed with 0.1 mL polytetrafluoroethylene (Teflon 60% wt. dispersion in water) and then applied on a carbon paper cut into the appropriate dimensions. The paste was first dried at 80 °C, and then, it was sintered at 340 °C. The procedure was repeated so as to deposit 0.5 mg of carbon black per cm². The active area of the electrode was 17.5 cm² (5 cm × 3.5 cm).

3.5. Apparatus and Measurements

The apparatus used for photoelectrochemical measurements and hydrogen production is schematically presented by Figure 1. It was made of two Pyrex cylinders separated by an ion transfer membrane (ROBU, Germany, porosity SGQ 5, diameter 25 mm, thickness 2 mm). One cylinder accommodated the photoanode and the reference electrode (Ag/AgCl) and the other the counter electrode. The counter electrode compartment was sealed using appropriate fittings, which allowed de-aeration of the solution by Ar flow, collection of the produced H₂, and counter electrode electric connection. The photoanode compartment was exposed to the ambient environment. The active area of the counter electrode was 3.5 × 5 cm², while the area of the photoanode was 1 × 1 cm² in the case of current-voltage measurements, but increased to 3.5 × 5 cm² in the case of hydrogen production. Each compartment was filled with 200 mL of 0.5 M NaClO₄. However, in the anode compartment, we also added 5% v/v ethanol. Illumination was made in all cases using a Xe lamp providing an intensity of 100 mW·cm⁻² at the position of the photoanode. Hydrogen was detected online by using Ar as the carrier gas and an SRI 8610C gas chromatograph. Calibration of the chromatograph signal was accomplished by comparison with a standard of 0.25% H₂ in Ar. Current-voltage curves and application of electric bias were accomplished with an Autolab potentiostat PGSTAT128N (Metrohm AG, Herisau, Switzerland)

4. Conclusions

This work demonstrated the improvement of the photoelectrocatalytic behavior and the increase of the hydrogen production rate by adding a titania film on the top of a WO₃ photoanode. The electrochemical characteristics of the photoanode were not modified by TiO₂ film addition, but the obtained photocurrent largely increased, while the quantity of hydrogen proportionally increased as well. This effect was mainly ascribed to the passivation of WO₃ surface states, thus decreasing the number of charge recombination sites. This result is in accordance with the observations described in [24]. Increased photocurrent (and hydrogen) production may additionally be ascribed to the TiO₂ light scattering effect.

Author Contributions: P.M.A.: investigation. I.P.: investigation. D.R.: investigation. P.L.: conceptualization.

Funding: This research received no external funding.

Conflicts of Interest: The authors declare no conflict of interest.

References

- Pan, L.; Vlachopoulos, N.; Hagfeldt, A. Directly Photoexcited Oxides for Photoelectrochemical Water Splitting. *ChemSusChem* **2019**, *12*, 4337–4352. [[CrossRef](#)]
- Sakata, T.; Kawai, T. Heterogeneous photocatalytic production of hydrogen and methane from ethanol and water. *Chem. Phys. Lett.* **1981**, *80*, 341–344. [[CrossRef](#)]
- Lianos, P. Production of electricity and hydrogen by photocatalytic degradation of organic wastes in a photoelectrochemical cell the concept of the Photofuelcell: A review of a re-emerging research field. *J. Hazard. Mater.* **2011**, *185*, 575–590. [[CrossRef](#)]

4. Lianos, P. Review of recent trends in a photoelectrocatalytic conversion of solar energy to electricity and hydrogen. *Appl. Catal. B. Environ.* **2017**, *210*, 235–254. [[CrossRef](#)]
5. Sfaelou, S.; Lianos, P. Photoactivated Fuel Cells (PhotoFuelCells). An alternative source of renewable energy with environmental benefits. *AIMS Mater. Sci.* **2016**, *3*, 270–288. [[CrossRef](#)]
6. Kondarides, D.I.; Daskalaki, V.M.; Patsoura, A.; Verykios, X.E. Hydrogen production by photo-induced reforming of biomass components and derivatives at ambient conditions. *Catal. Lett.* **2008**, *122*, 26–32. [[CrossRef](#)]
7. Yao, T.; An, X.; Han, H.; Chen, J.Q.; Li, C. Photoelectrocatalytic Materials for Solar Water Splitting. *Adv. Energy Mater.* **2018**, *8*, 1800210. [[CrossRef](#)]
8. Li, Z.; Luo, W.; Zhang, M.; Feng, J.; Zou, Z. Photoelectrochemical Cells for Solar Hydrogen Production: Current State of Promising Photoelectrodes, Methods to Improve Their Properties, and Outlook. *Energy Environ. Sci.* **2013**, *6*, 347–370. [[CrossRef](#)]
9. Shen, S.; Chen, J.; Wang, M.; Sheng, X.; Chen, X.; Feng, X.; Mao, S.S. Titanium dioxide nanostructures for photoelectrochemical applications. *Prog. Mater. Sci.* **2018**, *98*, 299–385. [[CrossRef](#)]
10. Jian, J.; Jiang, G.; van de Krol, R.; Wei, B.; Wang, H. Recent advances in rational engineering of multinary semiconductors for photoelectrochemical hydrogen generation. *Nano Energy* **2018**, *51*, 457–480. [[CrossRef](#)]
11. Kalanur, S.S.; Duy, L.T.; Seo, H. Recent Progress in Photoelectrochemical Water Splitting Activity of WO_3 Photoanodes. *Top. Catal.* **2018**, *61*, 1043–1076. [[CrossRef](#)]
12. Gratzel, M. Photoelectrochemical cells. *Nature* **2001**, *414*, 338–344. [[CrossRef](#)] [[PubMed](#)]
13. Liu, X.; Wang, F.; Wang, Q. Nanostructure-based WO_3 photoanodes for photoelectrochemical water splitting. *Phys. Chem. Chem. Phys.* **2012**, *14*, 7894–7911. [[CrossRef](#)] [[PubMed](#)]
14. Hodes, G.; Cahen, D.; Manassen, J. Tungsten Trioxide as a Photoanode for a Photoelectrochemical Cell (PEC). *Nature* **1976**, *260*, 312–313. [[CrossRef](#)]
15. Ashokkumar, M.; Maruthamuthu, P. Photocatalytic Hydrogen Production with Semiconductor Particulate Systems: An Effort to Enhance the Efficiency. *Int. J. Hydrogen Energy* **1991**, *16*, 591–595. [[CrossRef](#)]
16. Alexander, B.D.; Kulesza, P.J.; Rutkowska, I.; Solarska, R.; Augustynski, J. Metal Oxide Photoanodes for Solar Hydrogen Production. *J. Mater. Chem.* **2008**, *18*, 2298–2303. [[CrossRef](#)]
17. Gan, J.; Lu, X.; Tong, Y. towards Highly Efficient Photoanodes: Boosting Sunlight-Driven Semiconductor Nanomaterials for Water Oxidation. *Nanoscale* **2014**, *6*, 7142–7164. [[CrossRef](#)]
18. Wang, S.C.; Tang, F.Q.; Wang, L.Z. Visible Light Responsive Metal Oxide Photoanodes for Photoelectrochemical Water Splitting: A Comprehensive Review on Rational Materials Design. *J. Inorg. Mater.* **2018**, *33*, 173–197.
19. Sfaelou, S.; Pop, L.C.; Monfort, O.; Dracopoulos, V.; Lianos, P. Mesoporous WO_3 photoanodes for hydrogen production by water splitting and PhotoFuelCell operation. *Int. J. Hydrogen Energy* **2016**, *40*, 5902–5907. [[CrossRef](#)]
20. Raptis, D.; Dracopoulos, V.; Lianos, P. Renewable energy production by photoelectrochemical oxidation of organic wastes using WO_3 photoanodes. *J. Hazard. Mater.* **2017**, *333*, 259–264. [[CrossRef](#)]
21. Pop, L.C.; Sfaelou, S.; Lianos, P. Cation adsorption by mesoporous titania photoanodes and its effect on the current-voltage characteristics of photoelectrochemical cells. *Electrochim. Acta* **2015**, *156*, 223–227. [[CrossRef](#)]
22. Sfaelou, S.; Raptis, D.; Dracopoulos, V.; Lianos, P. BiOI solar cells. *RSC Adv.* **2015**, *5*, 95813–95816. [[CrossRef](#)]
23. Choi, T.; Kim, T.-S.; Kim, J.H. Transparent nitrogen doped TiO_2/WO_3 composite films for self-cleaning glass applications with improved photodegradation activity. *Adv. Powder Technol.* **2016**, *27*, 347–353. [[CrossRef](#)]
24. Yang, M.; He, H.; Zhang, H.; Zhong, X.; Dong, F.; Ke, G.; Chen, Y.; Du, J.; Zhou, Y. Enhanced photoelectrochemical water oxidation on WO_3 nanoflake films by coupling with amorphous TiO_2 . *Electrochim. Acta* **2018**, *283*, 871–881. [[CrossRef](#)]
25. Huang, W.; Wang, J.; Bian, L.; Zhao, C.; Liu, D.; Guo, C.; Yang, B.; Cao, W. Oxygen vacancy induces self-doping effect and metalloid LSPR in non-stoichiometric tungsten suboxide synergistically contributing to the enhanced photoelectrocatalytic performance of $\text{WO}_{3-x}/\text{TiO}_{2-x}$ heterojunction. *Phys. Chem. Chem. Phys.* **2018**, *20*, 17268–17278. [[CrossRef](#)]
26. Zeng, Q.; Bai, J.; Li, J.; Xia, L.; Zhou, B.; Sun, Y. Highly-stable and efficient photocatalytic fuel cell based on an epitaxial $\text{TiO}_2/\text{WO}_3/\text{W}$ nanothorn photoanode and enhanced radical reactions for simultaneous electricity production and wastewater treatment. *Appl. Energy* **2018**, *220*, 127–137. [[CrossRef](#)]

27. Guaraldo, T.T.; Goncales, V.R.; Silva, B.F.; de Torresi, S.I.C.; Zanoni, M.V.B. Hydrogen production and simultaneous photoelectrocatalytic pollutant oxidation using a TiO₂/WO₃ nanostructured photoanode under visible light irradiation. *J. Electroanal. Chem.* **2016**, *765*, 188–196. [[CrossRef](#)]
28. Georgieva, J.; Valova, E.; Armyanov, S.; Philippidis, N.; Poulios, I.; Sotiropoulos, S. Bi-component semiconductor oxide photoanodes for the photoelectrocatalytic oxidation of organic solutes and vapours: A short review with emphasis to TiO₂-WO₃ photoanodes. *J. Hazard. Mater.* **2012**, *211*, 30–46. [[CrossRef](#)]
29. Georgieva, J.; Armyanov, S.; Poulios, I.; Sotiropoulos, S. An all-solid photoelectrochemical cell for the photooxidation of organic vapours under ultraviolet and visible light illumination. *Electrochim. Commun.* **2019**, *11*, 1643–1646.
30. Patel, P.P.; Ghadge, S.D.; Hanumantha, P.J.; Datta, M.K.; Gattu, B.; Shanthi, P.M.; Kumpta, P.N. Active and robust novel bilayer photoanode architectures for hydrogen generation via direct non-electric bias induced photo-electrochemical water splitting. *Int. J. Hydrogen Energy* **2018**, *43*, 13158–13176. [[CrossRef](#)]
31. Kalamaras, E.; Lianos, P. Current Doubling effect revisited: Current multiplication in a PhotoFuelCell. *J. Electroanal. Chem.* **2015**, *751*, 37–42. [[CrossRef](#)]
32. Doukas, E.; Balta, P.; Raptis, D.; Avgouropoulos, G.; Lianos, P. A Realistic Approach for Photoelectrochemical Hydrogen Production. *Materials* **2018**, *11*, 1269. [[CrossRef](#)] [[PubMed](#)]
33. Murau, P.C. Dissolution of Tungsten by Hydrogen Peroxide. *Anal. Chem.* **1961**, *33*, 1125–1126.
34. Orel, B.; Krasovec, U.O.; Groselj, N.; Kosec, M.; Drazi, G.; Reisfeld, R. Gasochromic Behavior of Sol-Gel Derived Pd Doped Peroxopolytungstic Acid (W-PTA) Nano-Composite Films. *J. Sol-Gel Sci. Technol.* **1999**, *14*, 291–308. [[CrossRef](#)]
35. Kudo, T. A New Heteropolyacid with Carbon as a Heteroatom in a Keggin-like Structure. *Nature* **1984**, *312*, 537–538. [[CrossRef](#)]
36. Ito, S.; Chen, P.; Comte, P.; Nazeeruddin, M.K.; Liska, P.; Pechy, P.; Gratzel, M. Fabrication of screen-printing pastes from TiO₂ powders for dye-sensitised solar cells. *Prog. Photovolt. Res. Appl.* **2007**, *15*, 603–612. [[CrossRef](#)]



© 2019 by the authors. Licensee MDPI, Basel, Switzerland. This article is an open access article distributed under the terms and conditions of the Creative Commons Attribution (CC BY) license (<http://creativecommons.org/licenses/by/4.0/>).